Journal of Industrial and Engineering Chemistry 80 (2019) 152–159

Contents lists available at ScienceDirect

Journal of Industrial and Engineering Chemistry

journal homepage: www.elsevier.com/locate/jiec

Correlation verification of process factors and harmful gas adsorption properties for optimization of physical activation parameters of PAN-based carbon fibers

Yun Jeong Choi[a,b,1], Ji Hong Kim[a,c,1], Ki Bong Lee[c], Young-Seak Lee[b], Ji Sun Im[a,d,*]

[a] Carbon Industry Frontier Research Center, Korea Research Institute of Chemical Technology (KRICT), Daejeon 34114, Republic of Korea
[b] Department of Chemical Engineering and Applied Chemistry, Chungnam National University, Daejeon 34134, Republic of Korea
[c] Department of Chemical Engineering and Applied Chemistry, Korea University, Seoul 02841, Republic of Korea
[d] University of Science and Technology (UST), Daejeon 34113, Republic of Korea

ARTICLE INFO

Article history:
Received 27 November 2018
Received in revised form 22 July 2019
Accepted 24 July 2019
Available online 30 July 2019

Keywords:
Activated carbon fiber
Steam activation
SO_2
DMMP
Pore structure

ABSTRACT

In this study, the effects of activation parameters in the steam activation of polyacrylonitrile-based carbon fibers on pore formation properties were investigated. The activation temperature was used as a primary parameter, and the activation time was adjusted for each condition to obtain similar levels of activation yields. Based on the activation yield of activated carbon fibers (ACFs), the activation energy was calculated as 142.2 kJ/mole. As a result of BET analysis, it was confirmed that the specific surface area and pore volume of ACFs were improved as the activation temperature was increased. The sample treated at 850 °C during 45 min showed a high specific surface area (1041.9 m^2/g) and a pore volume (0.49 cm^3/g). This developed pore structures improved the gas adsorption properties of ACFs.

Introduction

Research on various adsorbents intended to adsorb and eliminate pollutants has been actively underway. Porous materials, including Al_2O_3, MOF (metal organic framework), zeolite, and activated carbon, are now being widely used as materials for adsorbents [1–7]. Among them, activated carbon is the most widely used because it provides high specific surface area and easy control of its internal pore structures [8,9].

Under the standards of the International Union of Pure and Applied Chemistry (IUPAC), pores are divided according to size into micropores with a diameter of 2 nm less, mesopores with diameters ranging from 2 to 50 nm, and macropores with a diameter of 50 nm or above [10]. Here, adsorption performance of each type of adsorbent varies depending on the target pollutant. In general, micropore materials are used for air cleaning and pollutants removal, while mesopore materials, such as activated carbon, are used for liquid adsorption applications, such as water purification [11–13].

Notably, using activated carbon comes with a risk of secondary contamination due to its long adsorption time and severe dust generation. Also, its broad distribution range of pore size in part limits its performance [14,15]. This limitation can be overcome with the application of activated carbon fibers. Activated carbon fibers have high specific surface area (~3000 m^2/g) and micropore fraction (~98%). Thus, they are more suitable for meteorological adsorption applications while providing much better adsorption properties in terms of speed and capacity [16–19].

These porous carbon materials are fabricated through an activation process. The activation process is divided into a physical activation method and chemical activation method according to the manufacturing method [20]. The physical activation method uses oxidizing gases, such as water vapor, carbon dioxide, and oxygen, to implement carbon gasification. In contrast, the chemical activation method uses acid and alkaline chemical agents, including KOH, NaOH, Na_2CO_3, and H_3PO_4, as activators, and its process temperature is lower than that of the physical method. Therefore, the chemical method is more suitable for fabricating activated carbon with high specific surface area [21,22]. The method, however, requires an additional sludge washing process, thereby resulting in a more complex manufacturing process and a higher risk of secondary contamination. On the other hand, the physical activation process is simpler and eco-friendly and does not incur environmental treatment costs, thereby reducing overall process costs.

* Corresponding author at: Carbon Industry Frontier Research Center, Korea Research Institute of Chemical Technology (KRICT), Daejeon 34114, Republic of Korea.
E-mail address: jsim@krict.re.kr (J.S. Im).
[1] Authors contributed equally to this work.

https://doi.org/10.1016/j.jiec.2019.07.044
1226-086X/

In the physical activation method, pore characteristics are determined by the gasification reaction that occurs during the activation process, and this gasification reaction leads to a decrease in activation yields. Changes in activation yields can be translated into the conversion rate of activated carbon fibers, and this approach makes it possible to implement a kinetics-based analysis of the activation process. A steam activation method is a process where H_2O, an oxidizing gas, is decomposed at high temperatures and interacts with carbon atoms contained in carbon fibers, and then gasified into gases, such as CO or H_2 [23]. The fundamental purpose of this process is to induce reactions between carbon fibers and oxygen atoms, and thus a kinetics equation that is used for oxidation can be employed here. Various studies on a kinetics-based analysis and the energy aspects of the oxidation process of carbon fibers have been carried out, but a few research result has been reported regarding the application of this kinetics equation to activation processes in attempts to implement a kinetics-based analysis of activation mechanisms [24–26].

The present study investigated changes in the pore structure of PAN-based carbon fibers during the physical activation process using steam, arising from the effect of process parameters (e.g., temperature and time). A kinetics-based analysis of the steam activation method of PAN-based carbon fibers was performed by deciding the main parameters based on consideration of quick oxidation at high temperature during physical activation. A new equation on decided parameters can be obtained based on kasaoka equation. Through these procedures, pore formation mechanisms of activated carbon fibers were investigated. Subsequently, to assess the developed activated carbon fibers with respect to their ability to adsorb harmful gases, adsorption characteristics tests were performed using sulfur oxides (SOx) and dimethyl methyl phosphonate (DMMP).

Experimental

Fabrication of PAN-based activated carbon fibers

In the present study, activated carbon fibers were fabricated using 50 g of PAN-based fibers (Kolon Industries Inc.) with a diameter of 10–11 μm., as follows: Those PAN-based fibers were oxidized (stabilized) at 230 °C for 4 h and carbonized at 900 °C for 1 h into PAN-based carbon fibers. Subsequently, these treated PAN-based carbon fibers were processed into PAN-based activated carbon fibers through the steam activation process.

In the steam activation process, N_2 gas was injected at a rate of 200 cc/min in an inert atmosphere. The heating rate to each activation temperature was set to 5 °C/min, and, when the set activation temperature (700, 750, 800, 850 °C) was reached, steam injection was started in a 17 L reactor at a rate of 200 ml/min. The steam generator was heated and maintained at 300 °C. Generated steam was directly injected into the reactor to induce intended reactions for a specific activation time. Details of the set reaction temperatures and time periods are shown in Table 1. At higher activation temperatures, the activation time was set to be shorter to obtain similar levels of activation yields.

Analysis of pore structure of activated carbon fibers

Adsorption-desorption isotherms of N2 gas were measured at 77 K using a specific surface area analyzer, and, based on these measurements, the specific surface area (S_{BET}, m^2/g) and total pore volume (V_T, cm^3/g) of the fabricated activated carbon fibers were estimated. Experimental specimens were pretreated at 200 °C for eight hours in a vacuum and subsequently subjected to N_2 adsorption and desorption. The specific surface area of these prepared specimens was measured using a multipoint-Brunauer–Emmett–Teller (BET) method, and the volume of micropores contained in the specimens was estimated using a t-plot method.

Table 1
Activation conditions and its yield.

Sample name	Activation condition		
	Temperature (°C)	Time (min)	Yield (wt%)
700 – 3 h	700	180	68.00
700 – 4 h		240	56.38
700 – 6 h		360	47.86
750 – 2 h	750	120	45.55
750 – 3 h		180	40.13
750 – 4 h		240	33.08
800 – 45 m	800	45	56.90
800 – 1 h		60	40.26
800 – 1 h 15 m		75	38.93
800 – 1 h 30 m		90	34.81
850 – 30 m	850	30	45.42
850 – 45 m		45	40.76
850 – 50 m		50	34.94
850 – 55 m		55	31.77

SO_2 adsorption test

SO_2 adsorption tests were performed on the fabricated activated carbon fibers using a multi-gas detector (Teledyne 7600). The cylindrical sample tube (diameter: 12 mm, height of 20 mm) was filled with 0.1 g of cut activated carbon fibers. And SO_2 gas (40.00 μmol/mol, RIGAS Co., Ltd., Republic of Korea) was passed through the tube at 500 cc/min. Subsequently, the outlet concentration of SO_2 gas was measured to estimate the degree of adsorption over time. The SO_2 adsorptivity of each specimen was calculated using the equations shown below [27].

$$V_{\text{eff}} = Q \cdot t_{\text{total}} \tag{1}$$

$$m = \frac{C_0 v_{\text{eff}}}{1000} \tag{2}$$

$$q = \frac{Q}{1000} \int_{t=0}^{t=t_{\text{total}}} C_0 dt \tag{3}$$

$$R_{\text{total}} = \frac{q_{\text{total}}}{m_{\text{total}}} \times 100 \tag{4}$$

Eq. (1) indicates the total volume of gas used, where Q (cc/min) refers to the flow rate and t_{total} (min) is the total amount of operation time. In Eq. (2), C_0 (mg/L) and m (mg) are the final concentration and total amount of SO_2 gas, flowed in through the porous tube, respectively. q (mg) in Eq. (3) is the amount of adsorption while R (%) in Eq. (4) is the gas adsorption rate. Aside from the equations above, when C/C_0 in the breakthrough curve is 0.05, the corresponding point and time are defined as the breakthrough point and breakthrough time (t_B), respectively. When C/C_0 is 0.95, the adsorption of each adsorbent was considered to be saturated, and the corresponding time is defined as the saturation time (t_S). The adsorption test was conducted at room temperature and 1 atm for 180 min.

DMMP adsorption test

To assess the DMMP adsorptivity of the fabricated activated carbon fibers, gas chromatography (6890 GC system, Hewlett-Packard) was applied. DMMP gas was produced by vaporizing a DMMP solution (97%, Sigma-Aldrich) and combining it with

high-purity nitrogen at a specific ratio. The DMMP gas concentration regulator and the ideal gas equation and other relevant equations used in the present study are shown in Fig. 1.

To be more specific, 0.019 g of the DMMP solution was combined with high-purity nitrogen (100 cc/min) under 101.33 KPa (1 bar) and at 150 °C into 104 ppm of DMMP gas, which was subsequently injected into the GC column (Porapak™, Porous Polymer Adsorbent matrix Porapak Q, 80–100 mesh). The injection of DMMP gas gave rise to GC peaks viewed in the display, and breakthrough curves were obtained by calculating the peak area of each GC peak. As in the SO_2 adsorption tests, the adsorptivity of each specimen was estimated using Eqs. (1)–(4) above [27].

Results and discussion

Kinetics mechanism of steam activation of PAN-based carbon fibers

Changes in activation yields depending on the activation temperature and time are shown in Fig. 2. To obtain similar levels of activation yields for each condition, the activation time period was set to be relatively long at low activation temperatures while the time was set to be relatively short at high temperatures. When activated at 700 °C, the activation yield remained at 47.86 wt% even after six hours. When activated at 750, 800, and 850 °C, it took 180, 60, and 45 min for the activation yield to reduce to 40 wt %, respectively. The slope of the activation yield-time curve tended to decrease more sharply as the activation temperature

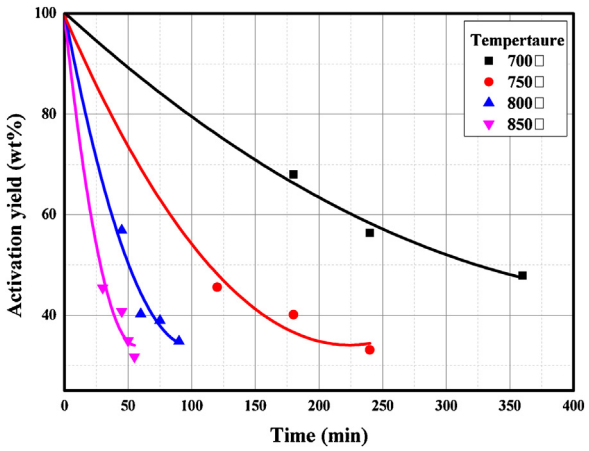

Fig. 2. The yields as a function of time and temperature in physical activation.

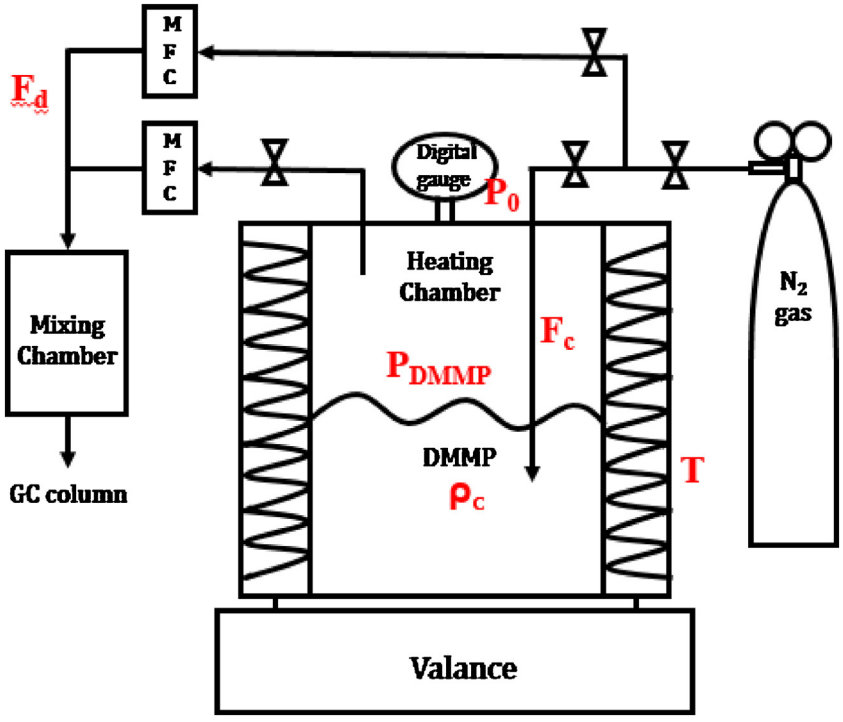

$$P_{DMMP} = \frac{\rho_c}{M}RT$$

$$F_{DMMP} = \left(\frac{P_{DMMP}}{P_0 - PDMM_P}\right)F_c$$

$$C_{DMMP} = \frac{10^6 F_{DMMP}}{F_d + Fc + FDMMP}$$

P_{DMMP} : Vapor pressure of DMMP
ρ_c : mass quantity of the DMMP
M : mass of per mole gas
R : ideal gas constant
T : temperature

F_{DMMP} : flow rate of DMMP
P_0 : total pressure
F_c : flow rate of carrier gas (N_2 gas)

C_{DMMP} : concentration of DMMP
F_d : flow rate of dilution gas (N_2 gas)

Fig. 1. DMMP gas concentration control equipment.

increased, and this implied that higher process temperatures would lead to the formation of more pore structures [28]. The effect of the activation process temperature on the specific surface area of each specimen will be described in 'Pore structure analysis of activated carbon fibers according to activation process conditions' section.

Based on these measurements, the correlation between the activation time and activation yield was characterized using the kinetics equation (by kasaoka), as shown in Eq. (5). Here, f refers to the conversion rate (%), and t (min) is the time [29]. When steam activation was applied, most of the yield reduction came from the gasification reaction of carbon atoms, and hence the conversion rate (f) was considered as the activation yield.

$$\exp\left(-at^{b}\right) = 1 - f \tag{5}$$

To make a linear relation between f and t, Eq. (5) was applied. Also, ln$a$, b, and r values were measured by plotting graphs for each activation temperature (700, 750, 800, and 850 °C), as summarized in Table 2. Here, ln$a$ refers to the x-intercept of the curve, and b is the slope of the curve. r is defined as the correlation coefficient, which indicates the degree of agreement between experimental data and the values obtained from the linear function. The closer to 1 the absolute value of the correlation coefficient r is, the higher the degree of agreement is. The selected four specimens showed a very high correlation of 0.92 or higher. K is the reaction rate constant, and it is assumed to follow the first order kinetics model.

Here, the reaction rate constant K is the average of the values obtained from Eq. (6) based on the calculated a and b values, as well as the activation yield data according to the activation temperature, as shown in Table 1 [30].

$$K(f) = a^{1/b\left[-\ln(1-f)^{(b-1)/b}\right]} \tag{6}$$

As a result, K values for each activation temperature, i.e., 700, 750, 800, and 850 °C, were determined to be 0.00219, 0.00541, 0.01295, and 0.02202, respectively. Simply put, the K values tend to increase with increasing activation temperature. This implies that the oxidation reaction proceeds more rapidly as the activation temperature increases. This approach based on the analysis of K values is expected to provide a reasonable prediction for the activation behavior and pore structure formation mechanism of PAN-based carbon fibers (Fig. 3).

The activation energy Ea was estimated using the Arrhenius equation, as shown in Eq. (7), based on the K values determined above.

$$\ln K = -\mathrm{Ea}/\mathrm{RT} + C(R = 8.314 \quad \mathrm{J/K} \quad \mathrm{mol}) \tag{7}$$

Eq. (7) can be converted into a linear function with a slope of $-\mathrm{Ea}/R$ by substituting $1/T$ with X and ln$K$ with Y. Here, the correlation coefficient was determined to be very high at 0.991. In Fig. 4, $-\mathrm{Ea}/R$ refers to the slope of the curve, and, based on the value, the activation energy of the steam activation process of the PAN-based carbon fibers was determined to be 142.2 kJ/mole.

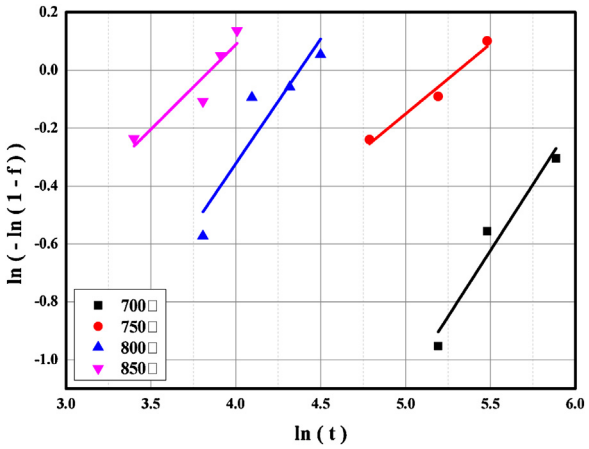

Fig. 3. '$Y - X$ plots' from '$Y = \ln a + b\,X$' for the PAN fiber during physical activation.

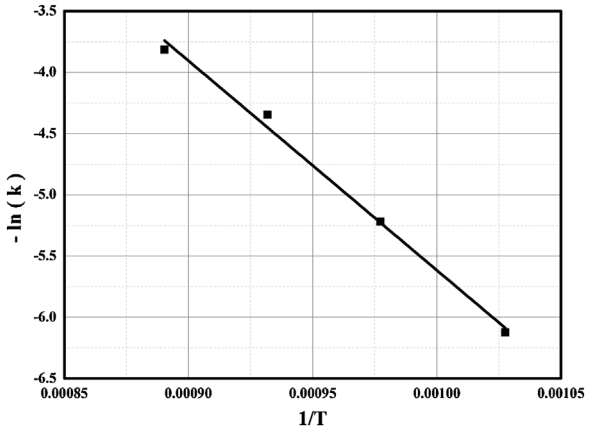

Fig. 4. Arrhenius plot of $-\ln K$ and $1/T$ for activation.

Pore structure analysis of activated carbon fibers according to activation process conditions

The BET analysis was performed to measure the specific surface area and pore volume of the activated carbon fibers fabricated through the steam activation method, and the results are shown in Fig. 5 and Table 3. As indicated above, the specific surface area tended to increase with increasing activation time at the same activation temperature. When the same activation time was applied, the specific surface area increased with increasing activation temperature, except in a specimen that was activated at 850 °C. These observations confirm that the activation time and temperature are factors affecting the activation characteristics of activated carbon fibers. Also, it was found that as the activation temperature increased, the specific surface area changed sharply even within the limited activation time. The specific surface area according to the activation temperate and time is plotted in Fig. 6.

Table 2
ln a, b and K calculated from '$Y = \ln a + b\,X$'.

Temperature (°CC)	ln a	b	K	r	Ea (kJ/mole)
700	−5.64742	0.91351	0.00219	0.97457	142.2
750	−2.57254	0.48427	0.00541	0.98564	
800	−3.77030	0.86189	0.01295	0.92898	
850	−2.25236	0.58515	0.02202	0.93939	

K: Reaction rate; r: Correlation coefficient.

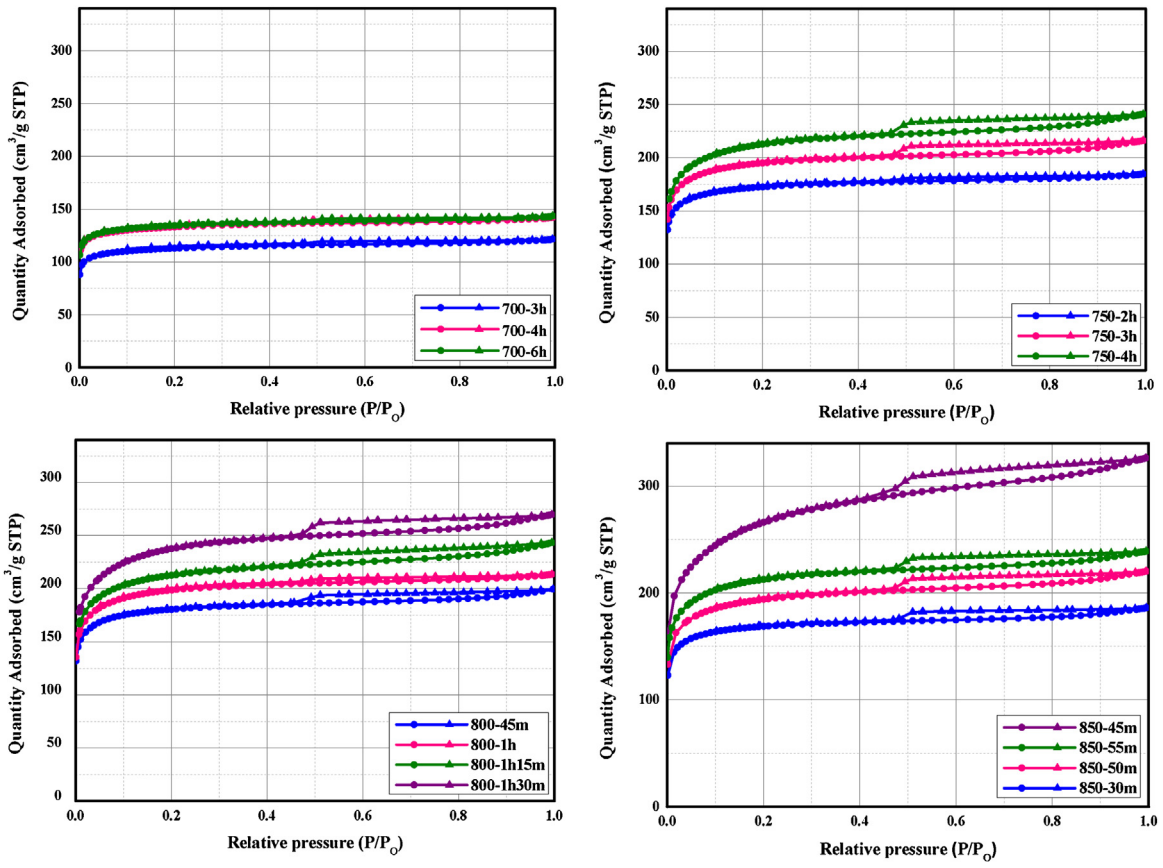

Fig. 5. Nitrogen adsorption isotherm on activated carbon prepared from the PAN fiber.

Table 3
Pore characteristics of the prepared activated carbon fiber.

Sample name	S_{BET} (m^2/g)	V_{micro} (cm^3/g)	V_{total} (cm^3/g)
700 – 3 h	448.4	0.17	0.19
700 – 4 h	528.7	0.20	0.21
700 – 6 h	535.5	0.20	0.22
750 – 2 h	677.9	0.26	0.29
750 – 3 h	759.5	0.29	0.33
750 – 4 h	816.3	0.32	0.37
800 – 45 m	707.4	0.27	0.31
800 – 1 h	770.1	0.30	0.33
800 – 1 h 15 m	817.2	0.32	0.38
800 – 1 h 30 m	902.3	0.36	0.42
850 – 30 m	662.5	0.26	0.29
850 – 45 m	1041.9	0.42	0.49
850 – 50 m	735.0	0.29	0.34
850 – 55 m	815.2	0.32	0.37

S_{BET}: BET surface specific area; V_{micro}: micropore volume; V_{total}: total pore volume.

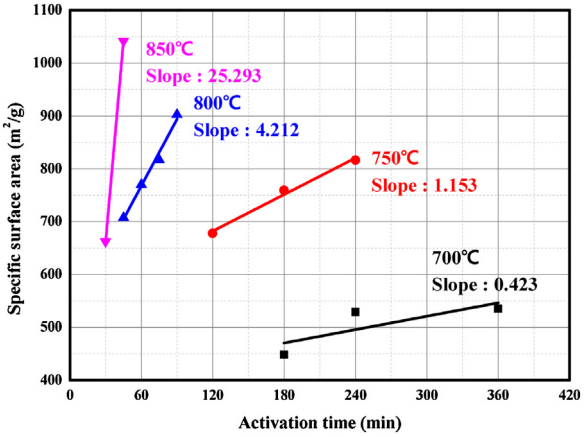

Fig. 6. Correlation between activation temperature/time and S_{BET}.

As shown in the graph, where the *x*-axis is the activation time and the *y*-axis is the S_{BET}, the slope of the curve tends to increase with increasing activation temperature. To be more specific, as the temperate increases, the curve shifts to the left (shorter activation time), but the specific surface area significantly increased. This implies that, between the two process parameters, the activation temperature is a more dominant factor than the activation time in determining the specific surface area.

Also, among the specimens activated in a temperature range between 700 and 800 °C, three sets of two specimens that showed similar levels of activation yields were selected and analyzed, as shown in Fig. 7: 700 – 6 h (47.86%) and 750 – 2 h (45.55%), 750 – 3 h (40.13%) and 800 – 1 h (40.26%), and 750 – 4 h (33.08%) and 800 – 1 h 30 m (38.93%). The comparison confirmed that the specific surface area was larger in the specimens that were treated at higher temperatures during a shorter period of time than in the specimens that were treated at lower temperatures for a longer period of time. In the meantime, the micropore volume was found to increase with increasing specific surface area. This phenomenon clearly indicated that the increase in the specific surface area was caused by the increased volume of micropores. This leads to the prediction that higher activation temperature is more suitable for the formation of microporous structures. Likewise, the activation

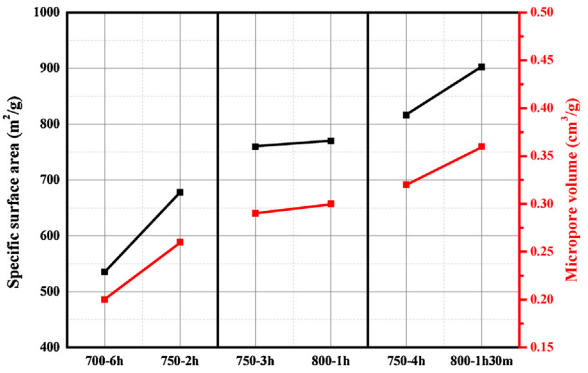

Fig. 7. Comparison of S_{BET}, V_{micro} of activated carbon fiber with similar activation yield.

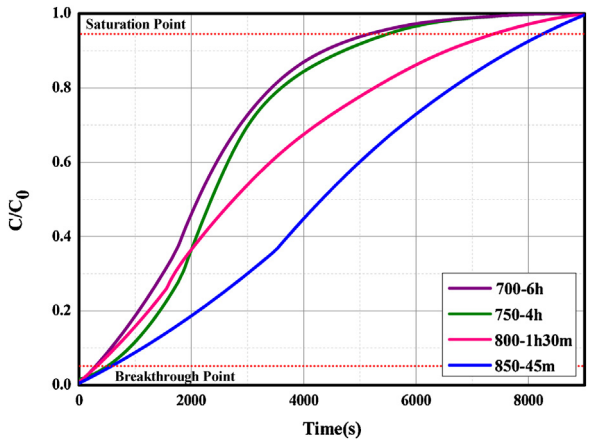

Fig. 8. SO_2 breakthrough curve of the prepared activated carbon fibers.

process of carbon fibers can be optimized by comparing the energy consumption depending on the activation temperature and time, and this approach will help reduce unit process costs.

In 'Kinetics mechanism of steam activation of PAN-based carbon fibers' section, it was shown that the oxidation reaction rate increases with increasing activation temperature. The actual activation test results verified that it was possible to fabricate activated carbon fibers with high specific surface area by increasing the activation temperature, even though the process time was relatively short. This result corresponds to the observed trend of the reaction rate constant *K*. In the specimen processed at 850 °C, however, the specific surface area decreased when the activation time exceeded 50 min. This phenomenon is considered to be due to the fact that the effect of the expansion and collapse of existing pores is greater than that of newly generated pores in the activation process [31]. It is also related to the reaction rate constant data, which represented the oxidation reaction of the PAN-based activated carbon fibers. The data showed that, at 850 °C, oxidation proceeded rapidly, which could be interpreted as the cause of the pore structure collapse. Therefore, in fabricating activated carbon fibers with high specific surface area, it is important to determine optimized activation conditions where excessive activation is prevented so that the pore structures are not collapsed.

SO_2 adsorption characteristics of fabricated activated carbon fibers

Based on the above measurements, four specimens with highest specific surface areas were selected and subjected to harmful gas adsorption tests: 700 – 6 h (535 m^2/g), 750 – 2 h (816.3 m^2/g), 800 – 1 h 30 m (902.3 m^2/g), and 850 – 45 m (1041.9 m^2/g).

The results of SO_2 adsorption tests of the four specimens are shown in Fig. 8. Here, the *x*-axis is the total adsorption time and the *y*-axis refers to the ratio of the detected SO_2 concentration to the final SO_2 concentration (C/C_0). The time when C/C_0 was 0.05 was defined as the breakthrough time (t_B) while the time when C/C_0 was 0.95 was defined as the saturation time (t_S), and these points are indicated in the corresponding breakthrough curves.

As can be seen in Fig. 8, the larger the area below the curve is, the more SO_2 remains unadsorbed. Using these breakthrough curves and Eqs. (1)–(4) above, the adsorption characteristics of each specimen were estimated, as shown in Table 4. The adsorption amount (q) increased in the order of 700 – 6 h (751.73 mg) < 750 – 4 h (817.08 mg) < 800 – 1 h 30 m (988.69 mg) < 850 – 45 m (1061.12 mg), and this result corresponds to the observed trend of the specific surface area. Therefore, the specific surface area is considered to be an important factor that affects the SO_2 adsorptivity, and, again, this leads to the confirmation that micropores affect the adsorption process. In other words, the SO_2 adsorption process observed in activated carbon fibers with microporous structures can be interpreted mainly as the result of a physical adsorption mechanism [32,33]. Based on general physical adsorption kinetic theory, it is noted that monolayer of SO_2 is formed on Langmuir adsorption model. In Fig. 8, the first inflection point might mean the completed monolayer of SO_2 on the carbon surface on interaction between adsorbate and adsorbent. And then further increase of SO_2 adsorption amount can be explained on BET equation on interaction among adsorbate SO_2 molecules. The adsorption is processed quickly with adsorption heat [2,3,34–36].

In general, the breakthrough time and saturation time can be used as indexes to evaluate the adsorptivity of gas. The breakthrough time of the fabricated specimens with respect to SO_2 gas adsorption was increased from 4.80 to 9.42 min as the specific surface area increased from 535.5 m^2/g (700 – 6 h) to 1041.9 m^2/g (850 – 45 m). In the meantime, the saturation time was increased from 88.02 to 138.6 min. This phenomenon is ascribed to the improved SO_2 adsorption properties of the carbon fibers arising from increases in their specific surface area and micropore volume.

Table 4
Adsorption characteristics of ACFs on SO_2 gas.

	Superficial velocity Q (cc/min)	Final concentration C_0 (mg/L)	Total time t_{total} (min)	Breakthrough time t_B (min)	Saturation time t_S (cc)	Effluent volume V_{eff} (cc)	Total amount of gas injected m_{total} (mg)	Total removal R_{total} (%)	Adsorption capacity q_{total} (mg)
700 – 6 h	500	38.37	150	4.80	88.02	75000	2878	26.12	751.73
750 – 4 h	500	37.61	150	8.22	93.12	75000	2821	28.97	817.08
800 – 1 h 30 m	500	36.88	150	5.15	124.63	75000	2766	35.74	988.69
850 – 45 m	500	28.92	150	9.42	138.6	75000	2169	48.92	1061.12

Table 5
Adsorption characteristics of ACFs on DMMP gas.

	Superficial velocity Q (cc/min)	Final concentration C_0 (mg/L)	Total time t_{total} (min)	Breakthrough time t_B (min)	Saturation time t_S (cc)	Effluent volume V_{eff} (cc)	Total amount of gas injected m_{total} (mg)	Total removal R_{total} (%)	Adsorption capacity q_{total} (mg)
700 – 6 h	100	94	130	10.87	98.19	13,000	1222	39.89	487.48
750 – 4 h	100	103	150	25.14	118.83	15,000	1545	50.67	782.90
800 – 1 h 30 m	100	99	180	50.06	145.01	18,000	1782	55.43	987.82
850 – 45 m	100	106	230	80.18	142.92	23,000	2438	46.59	1135.9

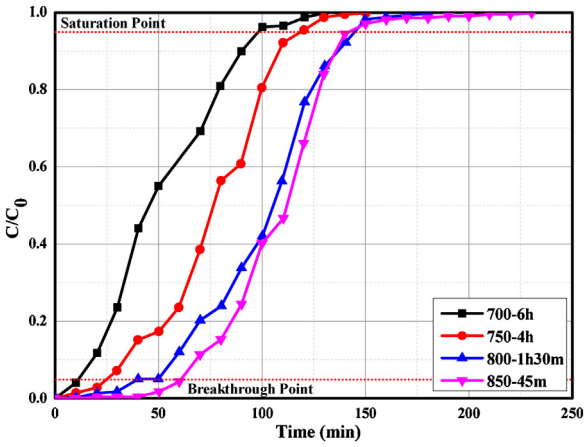

Fig. 9. DMMP breakthrough curve of the prepared activated carbon fibers.

DMMP adsorption characteristics of fabricated activated carbon fibers

The DMMP adsorptivity test results of the fabricated activated carbon fibers are shown in Fig. 9. Also, their adsorption properties were calculated using Eqs. (1)–(4), as summarized in Table 5. The DMMP adsorption amount (q) increased in the order of 700 – 6 h (487.48 mg) < 750 – 4 h (782.90 mg) < 800 – 1 h 30 m (987.82 mg) < 850 – 45 m (1135.9 mg), which corresponds to the results of the SO_2 adsorption tests. Again, this confirms that the DMMP adsorption process is also related to the microporous structure of activated carbon fibers, which allows a physical adsorption mechanism.

The breakthrough time was increased from 10.87 to 80.18 min as the specific surface area increased from 535.5 m^2/g (700 – 6 h) to 1041.9 m^2/g (850 – 45 m). In the meantime, the saturation time was increased from 98.19 to 142.92 min. Here, it should be noted that, in the 850 – 45 m specimen, the difference between the breakthrough time and saturation time was only 62.74 min, about 70% of the average. This phenomenon is also related to micropores contained in activated carbon fibers [32], i.e., due to the higher micropore volume in this specimen.

Conclusions

In the present study, the effects of activation process parameters in the steam activation process of PAN (polyacrylonitrile)-based carbon fibers on the pore formation mechanism were investigated. The Arrhenius equation was used to implement the kinetics-based analysis of the steam activation of these PAN-based carbon fibers. As a result, the activation energy was estimated to be 142.2 kJ/mole. In the meantime, the correlation coefficient was determined to be very high at 0.991, and it was also confirmed that the activation rate increased with increasing activation temperature. The pore structure of these carbon fibers was characterized by using a Brunauer–Emmett–Teller (BET) method, and the results confirmed that, between the two process parameters, the activation temperature was a more dominant factor than the activation time in determining the specific surface area and micropore volume. In all activated carbon fibers, the specific surface area and micropore volume tended to increase with increasing activation temperature. The maximum specific surface area was 1041.9 m^2/g, and the maximum micropore volume was 0.42 cm^3/g. Also, SO_2 and DMMP adsorption tests of the fabricated carbon fibers were performed, and, as a result, the absorptivity was determined to be 1061.12 mg for SO_2 gas and 1135.9 mg for DMMP gas.

Acknowledgments

This work was supported by the Korea Institute of Energy Technology Evaluation and Planning (KETEP) and the Ministry of Trade, Industry & Energy (MOTIE) of the Republic of Korea (No. 20181110200070, Functional porous composite for mitigating air pollutant by using coal combustion products) and also supported by the Korea Research Institute of Chemical Technology (KRICT) (No. KK1913-10, Fabrication of petroleum pitch based carbon absorbent for removal of hazardous air pollutants (SOx/NOx)).

References

[1] T. Hamzehlouyan, C.S. Sampara, J. Li, A. Kumar, W.S. Epling, Appl. Catal. B Environ. 181 (2016) 587–598, doi:http://dx.doi.org/10.1016/j.apcatb.2015.08.003.
[2] M.R. Hudson, W.L. Queen, J.A. Mason, D.W. Fickel, R.F. Lobo, C.M. Brown, J. Am. Chem. Soc. 134 (2012) 1970–1973, doi:http://dx.doi.org/10.1021/ja210580b.
[3] H. Deng, H. Yi, X. Tang, H. Liu, X. Zhou, Ind. Eng. Chem. Res. 52 (2013) 6778–6784, doi:http://dx.doi.org/10.1021/ie303319f.
[4] S. Han, Y. Huang, T. Watanabe, S. Nair, K.S. Walton, D.S. Sholl, J.C. Meredith, Microporous Mesoporous Mater. 173 (2013) 86–91, doi:http://dx.doi.org/10.1016/j.micromeso.2013.02.002.
[5] A.C. Elder, S. Bhattacharyya, S. Nair, T.M. Orlando, J. Phys. Chem. C 122 (2018) 10413–10422, doi:http://dx.doi.org/10.1021/acs.jpcc.8b00999.
[6] Y. Li, Y. Guo, T. Zhu, S. Ding, J. Environ. Sci. 43 (2016) 128–135, doi:http://dx.doi.org/10.1016/j.jes.2015.08.022.
[7] H. Yi, Z. Wang, H. Liu, X. Tang, D. Ma, S. Zhao, B. Zhang, F. Gao, Y. Zuo, J. Chem. Eng. Data 59 (2014) 1556–1563, doi:http://dx.doi.org/10.1021/je4011135.
[8] M. Asadullah, I. Jahan, M.B. Ahmed, P. Adawiyah, N.H. Malek, M.S. Rahman, J. Ind. Eng. Chem. 20 (2014) 887–896, doi:http://dx.doi.org/10.1016/j.jiec.2013.06.019.
[9] S. Jiang, L. Zhang, T. Chen, G. Wang, J. Ind. Eng. Chem. 20 (2014) 1693–1696, doi:http://dx.doi.org/10.1016/j.jiec.2013.08.018.
[10] A. Watanabe, T. Iiyama, K. Kaneko, Chem. Phys. Lett. 305 (1999) 71–74, doi:http://dx.doi.org/10.1016/S0009-2614(99)00362-0.
[11] M. Suzuki, Carbon 32 (1994) 577–586, doi:http://dx.doi.org/10.1016/0008-6223(94)90075-2.
[12] X. Zhang, B. Gao, A.E. Creamer, C. Cao, Y. Li, J. Hazard. Mater. 338 (2017) 102–123, doi:http://dx.doi.org/10.1016/j.jhazmat.2017.05.013.
[13] J.A. Arcibar-Orozco, J.R. Rangle-Mendez, P.E. Diaz-Flores, Water Air Soil Pollut. 226 (2015) 2197–2207, doi:http://dx.doi.org/10.1007/s11270-014-2197-1.
[14] S.G. Kim, Y.R. Chang, J. Korean Soc. Atmos. Environ. 24 (2008) 220–228, doi:http://dx.doi.org/10.5572/KOSAE.2008.24.2.220.
[15] H.S. Lim, M.J. Kim, E.Y. Kong, J.D. Jeong, Y.S. Lee, Appl. Chem. Eng. 29 (2018) 312–317, doi:http://dx.doi.org/10.14478/ace.2018.1007.
[16] Y.N. Prajapati, B. Bhaduri, H.C. Joshi, A. Srivastava, N. Verma, Chemosphere 155 (2016) 62–69, doi:http://dx.doi.org/10.1016/j.chemosphere.2016.04.040.

[17] X. Ma, H. Yang, L. Yu, Y. Chen, Y. Li, Materials 7 (2014) 4431–4441, doi:http://dx.doi.org/10.3390/ma7064431.
[18] Q.S. Liu, T. Zheng, P. Wang, J.P. Jiang, N. Li, Chem. Eng. J. 157 (2010) 348–356, doi:http://dx.doi.org/10.1016/j.cej.2009.11.013.
[19] S. Lei, J.I. Miyamoto, H. Kanoh, Y. Nakahigashi, K. Kaneko, Cabon 44 (2006) 1884–1890, doi:http://dx.doi.org/10.1016/j.carbon.2006.02.028.
[20] N. Diez, P. Alvarez, M. Granda, C. Blanco, R. Santamaria, R. Menendez, Chem. Eng. J. 15 (2015) 463–468, doi:http://dx.doi.org/10.1016/j.cej.2014.08.104.
[21] J. Li, D.H.L. Ng, P. Song, C. Kong, Y. Song, P. Yang, Biomass Bioenergy 75 (2015) 189–200, doi:http://dx.doi.org/10.1016/j.biombioe.2015.02.002.
[22] M.A. Lillo-Rodenas, D. Cazorla-Amoros, A. Linares-Solano, Carbon 41 (2003) 267–275, doi:http://dx.doi.org/10.1016/S0008-6223(02)00279-8.
[23] J.F. Gonzalez, S. Roman, C.M. Gonzalez-Garcia, J.M.V. Nabais, A.L. Ortiz, Ind. Eng. Chem. Res. 48 (2009) 7474–7481, doi:http://dx.doi.org/10.1021/ie801848.
[24] N.A. Rashidi, S. Yusup, B.H. Hameed, Energy 61 (2013) 440–446, doi:http://dx.doi.org/10.1016/j.energy.2013.08.050.
[25] K. Mahmoudi, K. Hosni, N. Hamdi, E. Srasra, Korean J. Chem. Eng. 32 (2015) 274–283, doi:http://dx.doi.org/10.1007/s11814-014-0216-y.
[26] I.A.W. Tan, B.H. Hameed, A.L. Ahmad, Chem. Eng. J. 127 (2007) 111–119, doi:http://dx.doi.org/10.1016/j.cej.2006.09.010.
[27] B.C. Bai, C.W. Lee, Y.S. Lee, Mater. Chem. Phys. 200 (2017) 361–367, doi:http://dx.doi.org/10.1016/j.matchemphys.2017.07.055.
[28] J. Pastor-Villegas, C.J. Duran-Valle, Carbon 40 (2002) 397–402, doi:http://dx.doi.org/10.1016/S0008-6223(01)00118-X.
[29] S. Kasaoka, Y. Sakata, S. Kayano, Y. Masuoka, Int. Chem. Eng. 23 (1983) 477.
[30] J.S. Roh, Carbon Lett. 9 (2008) 121–126, doi:http://dx.doi.org/10.5714/CL.2008.9.2.121.
[31] T. Yang, A.C. Lua, J. Colloid Interface Sci. 267 (2003) 408–417, doi:http://dx.doi.org/10.1016/S0021-9797(03)00689-1.
[32] Y.C. Chiang, P.C. Chiang, C.P. Huang, Carbon 39 (2001) 523–534, doi:http://dx.doi.org/10.1016/S0008-6223(00)00161-5.
[33] E. Atanes, A. Nieto-Marquez, A. Cambra, M.C. Ruiz-Perez, F. Fernandez-Martinez, Chem. Eng. J. 15 (2012) 60–67, doi:http://dx.doi.org/10.1016/j.cej.2012.09.043.
[34] S.H. Park, M.S. Choi, H.S. Park, Carbon Lett. (2019), doi:http://dx.doi.org/10.1007/s42823-019-00025-z.
[35] G.B. Lee, J.E. Park, S.Y. Hwang, J.H. Kim, S.H. Kim, H. Kim, B.U. Hong, Carbon Lett. (2019), doi:http://dx.doi.org/10.1007/s42823-019-00030-2.
[36] S.W. Seo, Y.J. Choi, J.H. Kim, J.H. Cho, Y.S. Lee, J.S. Im, Carbon Lett. (2019), doi:http://dx.doi.org/10.1007/s42823-019-00028-w.